Joule

CellPress

Article

Single-Junction Organic Solar Cell with over 15% Efficiency Using Fused-Ring Acceptor with Electron-Deficient Core

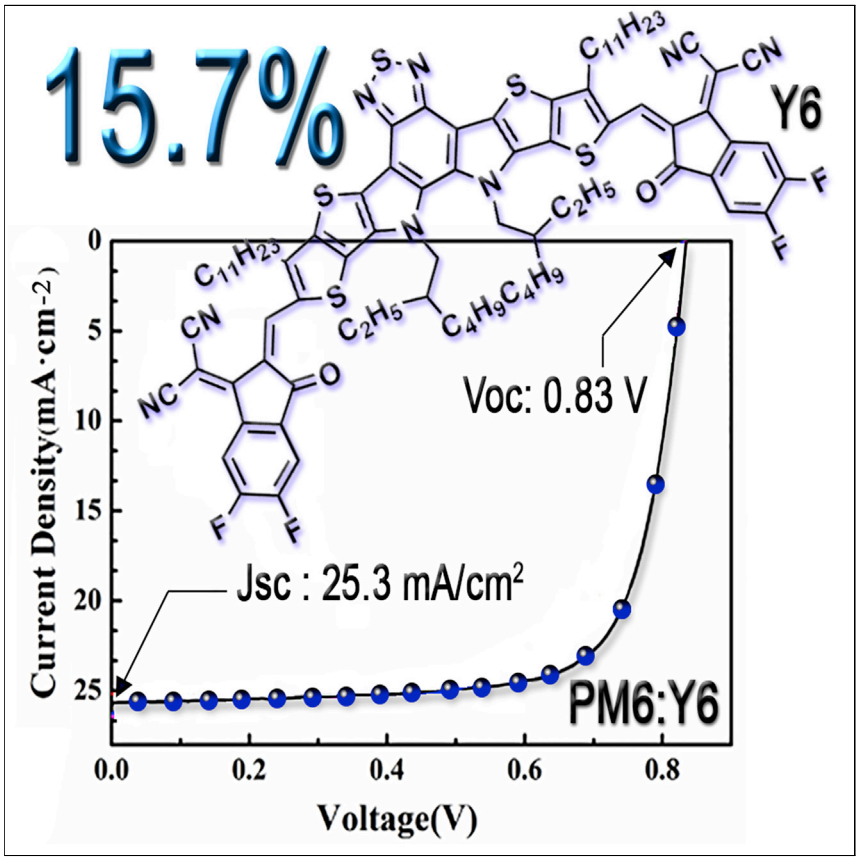

A new class of non-fullerene acceptor, Y6, by employing a ladder-type electron-deficient-core-based central fused ring with a benzothiadiazole core is reported. Organic photovoltaics made from Y6 in conventional and inverted architectures each exhibited a high efficiency of 15.7%, measured in two separate labs. Inverted device structures certified at Enli Tech Laboratory demonstrated an efficiency of 14.9%. Y6-based devices maintained the efficiency of 13.6% with an active layer thickness of 300 nm.

Jun Yuan, Yunqiang Zhang, Liuyang Zhou, ..., Jacek Ulanski, Yongfang Li, Yingping Zou

yingpingzou@csu.edu.cn

HIGHLIGHTS

An electron-deficient-core-based fused ring acceptor with benzothiadiazole unit

Conventional and inverted devices each exhibit a high efficiency of 15.7%

The certified efficiency of 14.9% has been demonstrated

Solar cells with an active layer thickness of 300 nm achieve the efficiency of 13.6%

Yuan et al., Joule 3, 1–12
April 17, 2019
https://doi.org/10.1016/j.joule.2019.01.004

Please cite this article in press as: Yuan et al., Single-Junction Organic Solar Cell with over 15% Efficiency Using Fused-Ring Acceptor with Electron-Deficient Core, Joule (2019), https://doi.org/10.1016/j.joule.2019.01.004

Joule

CellPress

Article

Single-Junction Organic Solar Cell with over 15% Efficiency Using Fused-Ring Acceptor with Electron-Deficient Core

Jun Yuan,[1] Yunqiang Zhang,[1] Liuyang Zhou,[1,2] Guichuan Zhang,[3] Hin-Lap Yip,[3] Tsz-Ki Lau,[4] Xinhui Lu,[4] Can Zhu,[1,2] Hongjian Peng,[1] Paul A. Johnson,[5] Mario Leclerc,[5] Yong Cao,[3] Jacek Ulanski,[6] Yongfang Li,[2] and Yingping Zou[1,7,*]

SUMMARY

Recently, non-fullerene *n*-type organic semiconductors have attracted significant attention as acceptors in organic photovoltaics (OPVs) due to their great potential to realize high-power conversion efficiencies. The rational design of the central fused ring unit of these acceptor molecules is crucial to maximize device performance. Here, we report a new class of non-fullerene acceptor, Y6, that employs a ladder-type electron-deficient-core-based central fused ring (dithienothiophen[3.2-b]- pyrrolobenzothiadiazole) with a benzothiadiazole (BT) core to fine-tune its absorption and electron affinity. OPVs made from Y6 in conventional and inverted architectures each exhibited a high efficiency of 15.7%, measured in two separate labs. Inverted device structures were certified at Enli Tech Laboratory demonstrated an efficiency of 14.9%. We further observed that the Y6-based devices maintain a high efficiency of 13.6% with an active layer thickness of 300 nm. The electron-deficient-core-based fused ring reported in this work opens a new door in the molecular design of high-performance acceptors for OPVs.

INTRODUCTION

In the last few decades, considerable progress has been made in the development of bulk-heterojunction (BHJ) organic photovoltaics (OPVs) based on a blend of a *p*-type organic semiconductor as donor and an *n*-type organic semiconductor (*n*-OS) as acceptor.[1–3] This is due to their low cost, light weight, and capability to be fabricated into flexible and semitransparent devices.[4–6] In general, to produce efficient OPVs, one needs donor and acceptor materials with high charge-carrier mobility, complementary absorption bands in the Vis-NIR range, and a small energy offset to minimize voltage losses.[7] The blend composition and morphology must also be optimized to maximize charge generation and transport.[8,9] Although one can increase the active layer thickness (for example, up to 300 nm) to improve light absorption, severe charge recombination could then occur that limits the fill factor (FF) of the devices due to increased distance of charge transport pathways.[10] In addition, most of the high-performance OPV materials absorb light with wavelength shorter than 800 nm,[11] which is not optimal for solar light utilization. In the last 2–3 years, rapid development of low-bandgap non-fullerene acceptors (NFAs) has provided effective ways to improve the performance of OPVs due to their tunable energy levels and strong absorption in the near-infrared region (NIR).[12–27] New acceptors have led to power conversion efficiencies (PCEs) over 13% when combined with a careful choice of polymeric donors.[28–34]

Context & Scale

Non-fullerene acceptors based organic photovoltaics (OPVs) have attracted considerable attention in the last decade due to their great potential to realize high-power conversion efficiencies. To achieve higher performance OPVs, the fundamental challenges are in enabling efficient charge separation/transport and a low voltage loss at the same time. Here, we have designed and synthesized a new class of non-fullerene acceptor, Y6, that employs an electron-deficient-core-based central fused ring with a benzothiadiazole core, to match with commercially available polymer PM6. By this strategy, the Y6-based solar cell delivers a high-power conversion efficiency of 15.7% with both conventional and inverted architecture. By this research, we provide new insights into employing the electron-deficient-core-based central fused ring when designing new non-fullerene acceptors to realize improved photovoltaic performance in OPVs.

Please cite this article in press as: Yuan et al., Single-Junction Organic Solar Cell with over 15% Efficiency Using Fused-Ring Acceptor with Electron-Deficient Core, Joule (2019), https://doi.org/10.1016/j.joule.2019.01.004

Along these lines, desired NFAs should have highest occupied molecular orbital (HOMO) and lowest unoccupied molecular orbital (LUMO) energy levels that are correctly positioned with respect to the energy levels of the used donor material. In this work, we choose the commercially available polymer PM6 (as illustrated in Figure 1D) as the donor,[35] which has a HOMO energy level of –5.56 eV and a LUMO energy level of –3.50 eV, as determined from cyclic voltammetry (CV). In order to maximize the open-circuit voltage (V_{oc}) and the short-circuit current density (J_{sc}), the HOMO levels of NFAs should be close to that of donor polymer together with adequate LUMO levels to achieve ideal optical bandgap derived from the Shockley-Queisser efficiency limit mode.[36]

Our acceptor's design is based on our recently reported strategy of using a ladder-type multi-fused ring with an electron-deficient core as a central unit that showed a narrow bandgap.[37] Moreover, electron affinity can be fine-tuned by the introduction of an electron-withdrawing moiety in the middle of the central core to create a charge-deficient region.[38] In this regard, one of the most commonly employed electron-poor units is 2, 1, 3-benzothiadiazole (BT).[39] Indeed, because of its commercial availability and sp^2-hybridized nitrogen atoms endowing electron-withdrawing character, BT has been popular in constructing low-bandgap conjugated materials and polymers.[40] Moreover, BT-based polymers can potentially offer highly efficient thick-active-layer OPVs due to their good mobility.[41] One can therefore consider using BT as a core of the central fused ring unit in high-performance NFAs.

Based on the above considerations, a new BT-core-based fused-unit dithienothiophen[3.2-b]-pyrrolobenzothiadiazole, TPBT, was designed. Then, a new NFA molecule based on the TPBT central unit, Y6 (2,2′-((2Z,2′Z)-((12,13-bis(2-ethylhexyl)-3,9-diundecyl-12,13-dihydro-[1,2,5]thiadiazolo[3,4-e]thieno[2,"3′′:4′,5′]thieno[2′,3′:4,5]pyrrolo[3,2-g]thieno[2′,3′:4,5]thieno[3,2-b]indole-2,10-diyl)bis(methanylylidene))bis(5,6-difluoro-3-oxo-2,3-dihydro-1H-indene-2,1-diylidene))dimalononitrile) (Figure 1A), was synthesized for photovoltaic applications. The fused TPBT central unit preserves conjugation along the length of the molecule, which allows tuning of the electron affinity. 2-(5,6-Difluoro-3-oxo-2,3-dihydro-1H-inden-1-ylidene)malononitrile (2FIC) units were used as flanking groups to enhance absorption and promote intermolecular interactions by forming noncovalent F···S and F···H bonds and, hence, facilitate charge transport.[42–44] Moreover, long alkyl side chains were introduced on the terminal of the central unit to increase the solubility of the resulting small-molecule acceptor. This strategy increases the solubility in common organic solvents for NFAs.[45] Optimized photovoltaic devices showed a PCE of up to 15.7%. These remarkable results demonstrate that Y6 is an excellent acceptor for high-efficiency OPVs.

RESULTS AND DISCUSSION

Synthesis and Characterization

As fully described in the Supplemental Experimental Procedures, Y6 can be easily synthesized in 4 steps (Scheme 1). Compound **3** was prepared through Stille couplings of compounds **1** and **2**. The ladder-type fused ring backbone (compound **4**) was obtained by the double intramolecular Cadogan reductive cyclization of compound **3** in the presence of triethyl phosphate, followed by the addition of 1-bromo-2-ethylhexane under alkaline conditions. The dialdehyde compound **5** was prepared by Vilsmeier-Haack reaction as an orange-red solid. The target small molecule Y6 was obtained through a Knoevenagel condensation of the compound **5** with 2FIC. Nuclear magnetic resonance (NMR) spectra and the high-resolution mass

[1]College of Chemistry and Chemical Engineering, Central South University, Changsha 410083, P.R. China

[2]Beijing National Laboratory for Molecular Sciences, Institute of Chemistry, Chinese Academy of Sciences, Beijing 100190, P.R. China

[3]Institute of Polymer Optoelectronic Materials and Devices, State Key Laboratory of Luminescent Materials and Devices, South China University of Technology, Guangzhou, 510640, P.R. China

[4]Department of Physics, The Chinese University of Hong Kong, New Territories, Hong Kong, P.R. China

[5]Department of Chemistry, Université Laval, Quebec City, QC G1V 0A6, Canada

[6]Department of Molecular Physics, Lodz University of Technology, Zeromskiego 116, 90-924 Lodz, Poland

[7]Lead Contact

*Correspondence: yingpingzou@csu.edu.cn

https://doi.org/10.1016/j.joule.2019.01.004

Please cite this article in press as: Yuan et al., Single-Junction Organic Solar Cell with over 15% Efficiency Using Fused-Ring Acceptor with Electron-Deficient Core, Joule (2019), https://doi.org/10.1016/j.joule.2019.01.004

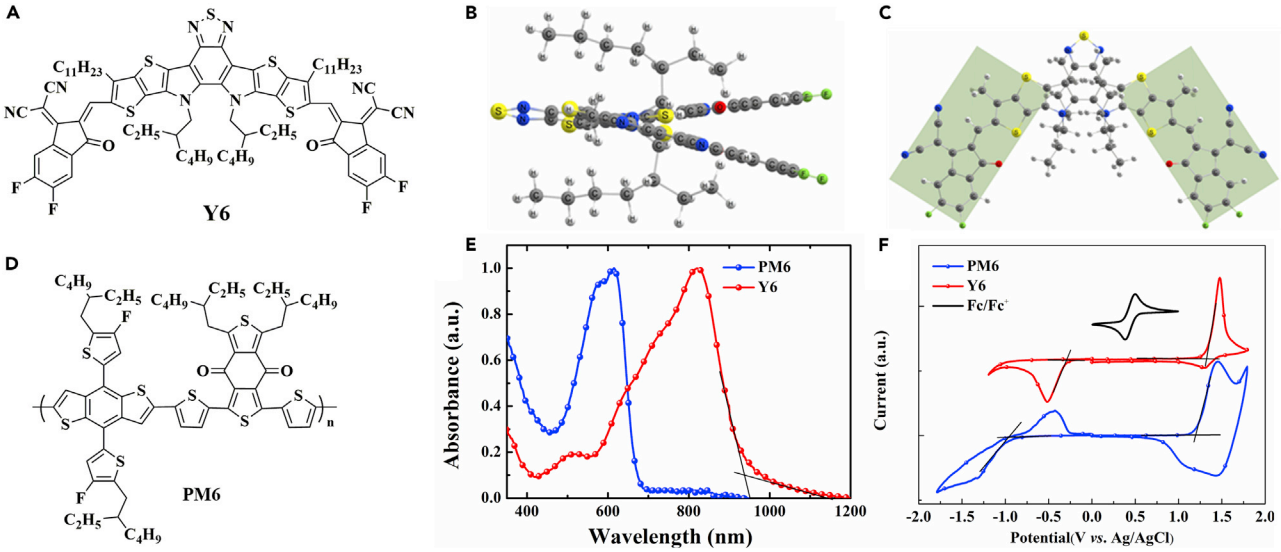

Figure 1. Molecular Structures and Photophysical Properties of Y6 and PM6

(A) Molecular structure of the acceptor Y6.

(B) Side view of the optimized geometry of Y6 computed with ωB97X-D/6-31+G(d,p).

(C) Top view of the optimized geometry of Y6 with ωB97X-D/6-31+G(d,p); planes are drawn to highlight the coplanar centers.

(D) Molecular structure of the donor PM6.

(E) Absorption spectra of thin films of PM6 and Y6.

(F) Energy diagrams of Y6 and PM6 in OPVs.

spectrum (MALDI-TOF) of the intermediates and Y6 are shown in Figures S1–S12. In order to better understand the 3D structure of Y6, density functional theory (DFT) calculations at the ωB97X-D/6-31+G (d,p) level were carried out with Gaussian 16 revision B.01.[46,47] To simplify the calculations, the alkyl side chains on the thiophene units were replaced by $-CH_3$ groups, but the whole 2-ethylhexyl side chains on the two nitrogen atoms were included. As shown in Figures 1B and 1C (side and top views, respectively), the acceptor consists of two planar units, with a twist in the center due to the alkyl groups attached to the nitrogens. This result in an N-C-C-N dihedral of –17.5 degree with the side chains on the nitrogen atoms orthogonal to the main plane. There is a C2 axis through the core of the molecule, and a degenerate structure exists with the core twisted in the opposite manner. There are three possible arrangements of the N-alkyl side chains, and the most stable has the two largest side chains directed toward the central core (Tables S4–S8). Without the need to synthesize spiro-like structures, the central conjugated core is sterically hindered to prevent over-aggregation with the presence of the alkyl side chains onto the nitrogen atoms while maintaining an intramolecular charge transport channel. Y6 is soluble in some common organic solvents such as chloroform and tetrahydrofuran at room temperature. Thermogravimetric analysis (TGA) (Figure S13) indicates Y6 has good thermal stability with decomposition temperatures at 318°C, which can meet the requirements of device fabrication. Figures 1E and S14 show the normalized absorption spectra of Y6 in chloroform solution and as thin film (corresponding optical data; Table S1). Compared to solution absorption spectrum, an important bathochromic shift of ~90 nm in the thin film indicates some aggregation of the molecular backbone and π-π interactions in the solid state. The absorption onset for Y6 is located at 931 nm, corresponding to an optical bandgap (E_g^{opt}) of 1.33 eV with an absorption coefficient of 1.07×10^5 cm^{-1} (Figure S15). As shown in Figure S16, the absorption maxima of PM6:Y6 blend film exhibits a small blue shift compared to the neat film of Y6. The post-treated blend film gives a small red shift, which might be

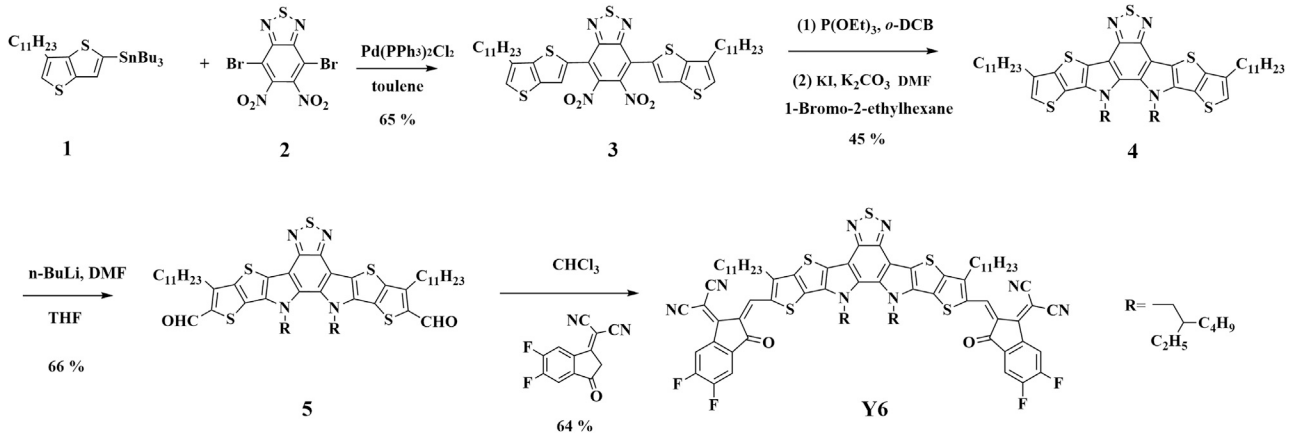

Scheme 1. Synthetic Routes for Y6

due to the changed morphology of blend film.[48] For the measurements of HOMO and LUMO energy levels of Y6, cyclic voltammetry was performed in anhydrous CH_3CN solution with Ag/AgCl as reference electrode and the ferrocene/ferrocenium (Fc/Fc^+) (0.436 eV versus Ag/AgCl) redox couple as internal reference. The results are collected in Table S1. From the results reported in Figure S17, the HOMO and LUMO energy levels of Y6 were estimated to be at –5.65 eV and –4.10 eV, respectively. As shown in Figure 1F, the small ΔE_{HOMO} offset (0.09 eV) between the PM6 donor and Y6 acceptor should be able to afford enough driving force for charge separation and maintain a low energy loss.[49,50]

Photovoltaic Properties

The Y6 molecule was applied as acceptor in BHJ-type organic solar cells with the medium bandgap (E_g^{opt} = 1.81 eV) conjugated polymer PM6 as *p*-type donor for complementary absorption with acceptor (Figure 1E), with the conventional device architecture of ITO/PEDOT:PSS/PM6:Y6/PDINO/Al. The fabrication conditions including the donor/acceptor weight ratios, blend film thickness, and thermal annealing in the active layer were carefully optimized. The key device parameters and all detailed photovoltaic data are summarized in Tables 1, S2, and S3. Devices based on the as-cast PM6:Y6 (1:1.2) blend achieved an impressive PCE of 15.3% with V_{oc} of 0.86 V, J_{sc} of 24.3 mA cm^{-2}, and an FF of 73.2%. On the basis of D:A weight ratio of 1:1.2, by thermal annealing at 110°C for 10 min, the PCE of the device decreased from 15.3% to 14.7% due to the decreased V_{oc} from 0.86 V to 0.84 V, although the device showed a slightly higher J_{sc}. Subsequently, the high boiling point processing additive 1-chloronaphthalene (CN) was used to optimize the morphology of the active layer. The result showed that the additive concentration of 0.5 wt% CN led to a PCE of 15.4% with a V_{oc} of 0.86 V, a J_{sc} of 23.86 mA cm^{-2}, and an FF of 75%. Figure 2A shows the best current density versus voltage (*J-V*) curve of the PM6:Y6-based device with the additive and thermal annealing treatment at 110°C for 10 min. This optimized device demonstrated a record high PCE of 15.7% with a higher J_{sc} of 25.3 mA cm^{-2} and an FF of 74.8%. When the active layer thickness increased to 250 nm, the Y6-based device still exhibits a high PCE of 14.1% with a notably even larger J_{sc} of 27.1 mA cm^{-2} but a slightly lower FF of 62.8% (Figure 2C). Upon a further increase of the thickness to 300 nm, a relatively higher PCE of 13.6% was still obtained with a J_{sc} of 26.5 mA cm^{-2} and an FF of 62.3%. Figure 2B shows the *EQE* spectra of the solar cells, and the maximum *EQE* plateau reached about 70%–80% from 450 to 830 nm. The integrated J_{sc} of the device based on

Please cite this article in press as: Yuan et al., Single-Junction Organic Solar Cell with over 15% Efficiency Using Fused-Ring Acceptor with Electron-Deficient Core, Joule (2019), https://doi.org/10.1016/j.joule.2019.01.004

Table 1. Photovoltaic Performance of the PM6:Y6 (1:1.2, *w/w*)-Based Devices (the Average Values for 10 Devices in the Brackets), under the Illumination of AM 1.5 G, 100 mW/cm^2

Device Type	Thickness (nm)	V_{OC} (V)	J_{SC} (mA cm^{-2})	FF (%)	PCE (%)
Conventional	150[a]	0.86	24.3	73.2	15.3 (15.2 ± 0.1)
	150[b]	0.83	25.3	74.8	15.7 (15.6 ± 0.1)
	200[b]	0.83	25.8	66.9	14.3 (14.2 ± 0.1)
	250[b]	0.82	27.1	62.8	14.1 (13.9 ± 0.2)
	300[b]	0.82	26.5	62.3	13.6 (13.3 ± 0.3)
Inverted	100[b]	0.82	25.2	76.1	15.7 (15.5 ± 0.2)
	100[c]	0.83	23.2	76.8	14.9

[a]As-cast.
[b]Under 0.5% chloronaphthalene (CN) with thermal annealing at 110°C for 10 min.
[c]The certified results from Enli Tech Optoelectronic Calibration Lab (an ISO-approved PV Efficiency Verification Laboratory in Taiwan) (aperture area: 3.99 mm^2).

PM6:Y6 from *EQE* spectra with AM 1.5 G reference spectrum is 24.6 mA cm^{-2}, which agrees quite well with the J_{sc} value from the *J-V* curve within a 4% mismatch.

The dependence of J_{sc} on light intensity (*P*) was measured to gain some insight into the photocurrent transport and charge recombination in the blend films.[51] If the bimolecular recombination is negligible in the devices, then the value of α in the relation $J_{sc} \propto P^{\alpha}$ tends to the limit 1. For the solvent and thermal-annealing treated devices, $\alpha = 0.99$, which is close to 1 and higher than that ($\alpha = 0.96$) of the as-cast device (Figure S18). These results indicate that there is almost no bimolecular recombination in the optimized devices, which agrees with the high J_{sc} and FF of the optimized devices.

We also fabricated inverted devices with the device structure of ITO/ZnO/PM6:Y6/MoO_3/Ag for better long-term ambient stability. Again, an excellent PCE of 15.7% with a remarkably high J_{sc} of 25.2 mA cm^{-2} and FF of 76.1% was achieved in the inverted solar cells. The internal quantum efficiency (*IQE*) of the Y6-based inverted devices (100 nm) has been calculated based on reflection and *EQE* (the integrated J_{sc} is 24.7 mA cm^{-2}) shown in Figure S19B; the *IQE* spectrum shows a very high value of over 80% in a range from 450 to 860 nm (Figure S19C). The high *IQE* curve suggests that most absorbed photons create charge carriers that are collected at the electrodes. To confirm the reliability of the high PCE of the PM6:Y6-based device, we sent the optimized inverted device to Enli Tech Optoelectronic Calibration Laboratory (an ISO-approved PV Efficiency Verification Laboratory in Taiwan) for certification (Figures S20 and S21). They measured a PCE of 14.9% (with a V_{oc} of 0.83 V, a J_{sc} of 23.2 mA cm^{-2}, and an FF of 76.8%). The photovoltaic parameters of the inverted devices are summarized in Table 1 and the *J-V* characteristics are shown in Figure S19A.

To elucidate the charge carrier mobilities in the OPV devices, we have determined electron and hole mobilities in the PM6:Y6 blends by the space charge limited current (SCLC) method.[52] We measured the charge carrier mobilities in neat Y6 film and PM6:Y6 blend film with different layer thicknesses as reported in Figure S22 and Tables S9 and S10. These results show that the charge mobility can increase with enhanced thicknesses, especially the electron mobility. The unbalanced charge transport property facilitates the formation of space-charge transportation, especially in thick-film devices, which limits their performance. Since the charge transport in the blend is also dependent on its morphology and orientation, we will discuss the charge transport in terms of morphology and orientation of blend films as follows.

Please cite this article in press as: Yuan et al., Single-Junction Organic Solar Cell with over 15% Efficiency Using Fused-Ring Acceptor with Electron-Deficient Core, Joule (2019), https://doi.org/10.1016/j.joule.2019.01.004

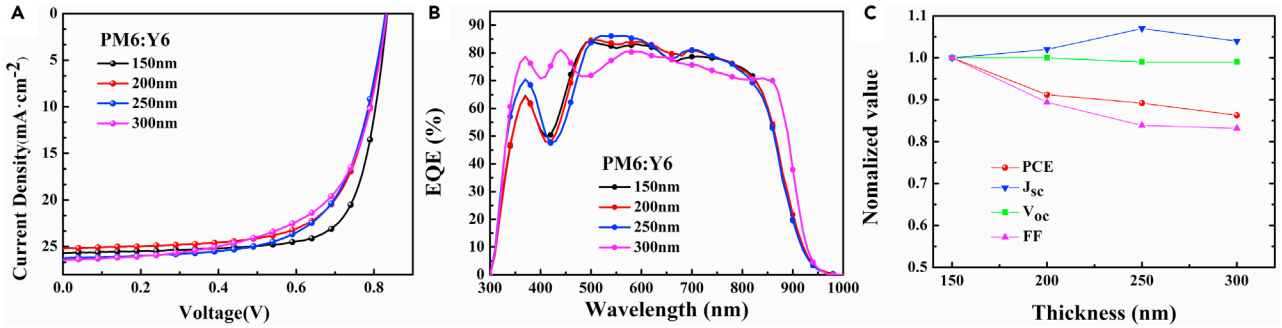

Figure 2. Photovoltaic Characteristics of the Y6-Based OPVs with Conventional Architectures

(A) *J-V* curve.

(B) *EQE* curve.

(C) Normalized value of all photovoltaic parameters with different active layer thickness.

Morphology Characterization

Grazing incidence wide-angle X-ray scattering (GIWAXS) was employed to investigate the bulk molecular packing information of neat and blend films. The 2D GIWAXS patterns of neat Y6 films, neat PM6, and blend PM6:Y6 are shown in Figures 3A–3C. The corresponding intensity profiles in the out-of-plane (OOP) and in-plane (IP) directions are presented in Figure 3D. The neat Y6 film (Figure 3A) exhibits a strong π-π stacking peak in the OOP direction at q = 1.76 Å^{-1} (d ~ 3.57 Å), indicating a preferential face-on orientation of Y6. Interestingly, there exist two diffraction peaks in the IP direction at q = 0.285 Å^{-1} (d ~ 21.9 Å) and 0.420 Å^{-1} (d ~ 15.0 Å), suggesting the co-existence of two distinct structure orders. Since one of them could be assigned to the lamellar peak, the other is mostly likely to originate from the backbone ordering due to the end-group π-π stacking, which was recently discovered in ITIC and ITIC-Th and facilitates the intermolecular electron transport.[53] The neat PM6 film (Figure 3B) presents a weaker π-π peak in the OOP direction at q = 1.68 Å^{-1} (d ~ 3.74 Å) and bimodal lamellar peaks in both IP and OOP directions at q = 0.300 Å^{-1} (d ~ 20.9 Å). The optimized blend PM6:Y6 film (Figure 3C) displays a strong diffraction peak in the OOP direction at q = 1.74 Å^{-1} (d ~ 3.61 Å), associated with the π-π stacking of Y6. In the IP direction, the scattering peak at q = 0.295 Å^{-1} (d ~ 21.3 Å) could be assigned to the lamellar stacking of either PM6 or Y6. The peak at q = 0.420 Å^{-1} (d ~ 15.0 Å), which was observed in the neat Y6, is still present, implying that the backbone ordering of Y6 is maintained in the blend PM6:Y6 film. GISAXS measurements were also carried out. The 2D GISAXS images and the in-plane scattering profiles are presented in Figure S23. q^{-4} dependence is used to fit the uplift in the small q (<0.006 Å^{-1}) regions due to scattering either from the surface roughness of the film or from the tail of a large amorphous regime. A fractal-like network model was adopted to account for the scattering contribution from the acceptor domain. The domain size of the Y6 phase in the optimized PM6:Y6 film was estimated to be 43.9 nm.

The morphologies were further investigated by atomic force microscopy (AFM) and transmission electron microscopy (TEM). The height images of the surface were observed by AFM for the blend films with different scan sizes (Figures 3E and S24), indicating good miscibility between PM6 and Y6. The root-mean-square (R_q) surface roughness value for the films is 0.93 nm. The phase separation was further visualized by TEM under the same conditions. As shown in Figures 3F and S25, the suitable nano-fibrillar structures in the blends suggest ideal phase separation between charge transport and recombination. These morphological features will in turn contribute to the remarkably high J_{sc}, *FF*, and PCE achieved by the devices.

Please cite this article in press as: Yuan et al., Single-Junction Organic Solar Cell with over 15% Efficiency Using Fused-Ring Acceptor with Electron-Deficient Core, Joule (2019), https://doi.org/10.1016/j.joule.2019.01.004

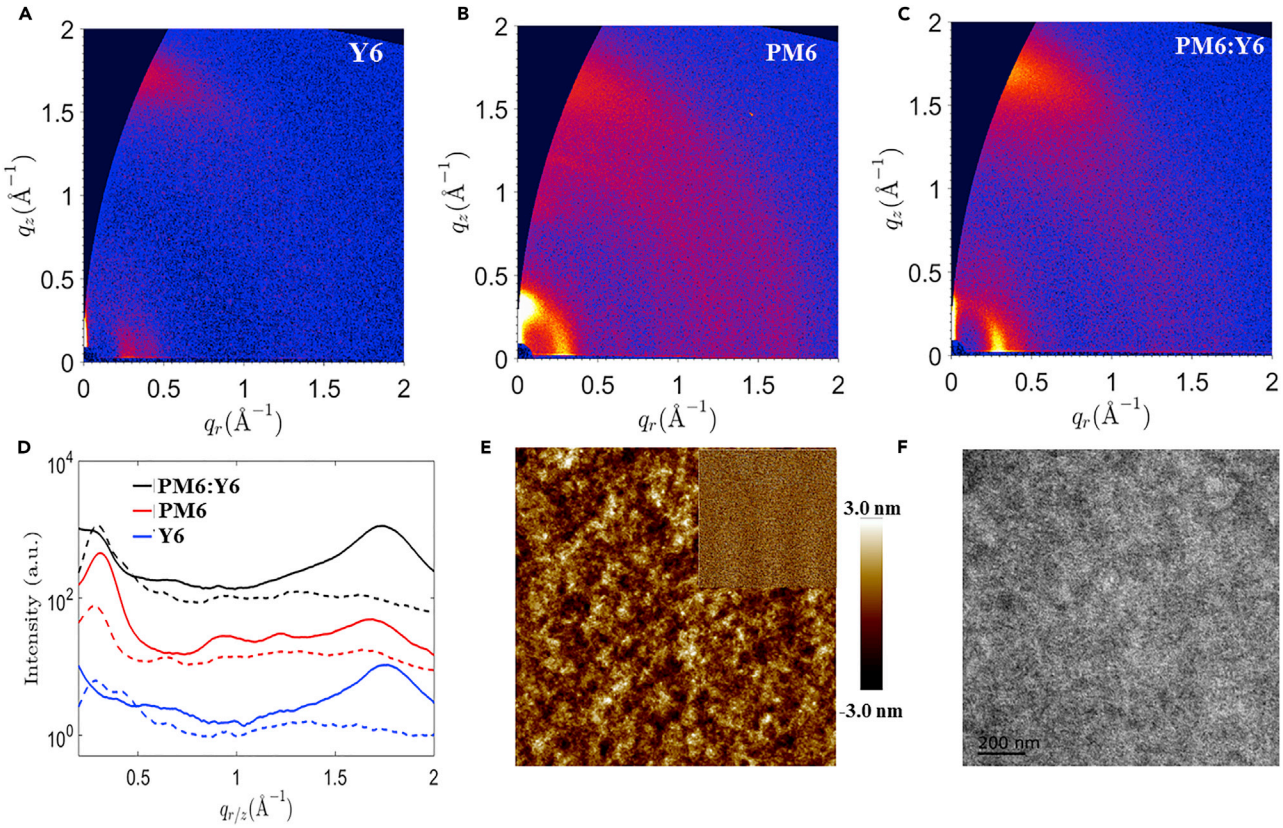

Figure 3. Film Morphologies

(A and B) GIWAXS images of neat Y6 and PM6.

(C) GIWAXS image of PM6:Y6 optimized blend films.

(D) GIWAXS intensity profiles along the in-plane (dotted line) and out-of-plane (solid line) directions.

(E) AFM images (5 μm × 5 μm) of PM6:Y6 optimized blend films.

(F) TEM image of PM6:Y6 optimized blend films.

Conclusion

In summary, we have designed and synthesized a new class of NIR-absorbing NFA (Y6) based on multi-fused ring central unit with electron-deficient benzothiadiazole core. The resulting electron affinity of Y6 combined with a low E_g^{opt} of 1.33 eV led to a record efficiency of 15.7% when blended with commercially available polymer PM6 donor for the devices with both conventional and inverted architecture. In addition, a certified PCE of 14.9% was obtained with an inverted device structure. More importantly, the Y6-based solar cells maintained a PCE of 14.1% and 13.6% with a thicker active layer of 250 nm and 300 nm, respectively. The high values of J_{sc}, exceeding 25 mA cm^{-2}, and high FF around 75% should result from the broad absorption and high charge carrier mobilities, high *IQE* in the range from 450 to 860 nm, and nano-segregated structure with preferred orientation. These results indicate that the electron-deficient-core-based fused ring reported in this work opens a new way in the molecular design of high-performance *n*-OS acceptors for OPVs.

EXPERIMENTAL PROCEDURES

Characterization of Materials

^{1}H NMR and ^{13}C NMR spectra were recorded using a Bruker AV-400 spectrometer in deuterated chloroform solution at 298 K, unless specified otherwise. Chemical shifts

Please cite this article in press as: Yuan et al., Single-Junction Organic Solar Cell with over 15% Efficiency Using Fused-Ring Acceptor with Electron-Deficient Core, Joule (2019), https://doi.org/10.1016/j.joule.2019.01.004

were reported as δ values (ppm) with tetramethylsilane (TMS) as the internal reference. The molecular mass was confirmed by using an Autoflex III matrix-assisted laser desorption ionization mass spectrometer (MALDI-TOF-MS). Thermogravimetric analysis (TGA) was conducted on a Perkin-Elmer TGA-7 with a heating rate of 20 K/min under nitrogen.

UV-Vis Absorption Spectra and Cyclic Voltammetry Measurement

UV-Vis absorption spectra were recorded on the SHIMADZU UV-2600 spectrophotometer. For the solid-state measurements, Y6 solutions in chloroform were spin-coated on quartz plates.

Cyclic voltammetry results were obtained with a computer-controlled CHI 660E electrochemical workstation using polymer or non-fullerene acceptor films on platinum (1.0 cm^2) as the working electrode, a platinum wire as the counter electrode, and Ag/AgCl (0.1 M) as the reference electrode in an anhydrous argon-saturated solution of 0.1 M tetrabutylammonium hexafluorophosphate (Bu_4NPF_6) in acetonitrile, at a scanning rate of 50 $mV \cdot s^{-1}$. Electrochemical onsets were determined at the position where the current started to rise from the baseline.

Fabrication and Characterization of the OPVs

OPVs were fabricated in the configuration of the traditional sandwich structure with an indium tin oxide (ITO) glass positive electrode and a PDINO/Al negative electrode in ICCAS. The ITO glass was pre-cleaned in an ultrasonic bath of detergent, deionized water, acetone, and isopropanol, and UV-treated in ultraviolet-ozone chamber (Jelight Company) for 15 min. A thin layer of PEDOT:PSS (poly(3,4-ethylene dioxythiophene): poly(styrene sulfonate)) (Baytron PVP Al 4083) was prepared by spin-coating the PEDOT:PSS solution filtered through a 0.45 μm poly(tetrafluoroethylene) (PTFE) filter at 3,000 rpm for 40 s on the ITO substrate. Subsequently, PEDOT:PSS film was baked at 150°C for 15 min in the air, and the thickness of the PEDOT:PSS layer was about 40 nm. The polymer PM6:Y6 (D:A = 1:1.2, 16 mg mL^{-1} in total) was dissolved in chloroform (CF) with the solvent additive of 1-chloronaphthalene (CN) (0.5%, v/v) and spin-cast at 3,000 rpm for 30 s onto the PEDOT:PSS layer. The thickness of the photoactive layer is about 150 nm measured by Ambios Technology XP-2 profilometer. A bilayer cathode consisting of PDINO (~15 nm) capped with Al (~150 nm) was thermally evaporated under a shadow mask with a base pressure of ca. 10^{-5} Pa. Finally, top electrodes were deposited in a vacuum onto the active layer. The active area of the device was 5 mm^2.

The inverted devices were fabricated and tested in SCUT. The ITO glass substrates were cleaned sequentially under sonication with acetone, detergent, deionized water, and isopropyl alcohol and then dried at 60°C in a baking oven overnight, followed by a 4-min oxygen plasma treatment. For inverted devices, a ZnO electron transport layer (a thickness of ~30 nm) was prepared by spin-coating at 5,000 rpm for 30 s from a ZnO precursor solution (diethyl zinc, 1.5 M solution in toluene purchased from Acros, diluting in tetrahydrofuran) on ITO substrates, followed by thermal annealing at 150°C for 30 min. The active layers were deposited as mentioned above; at a vacuum level of 1×10^{-7} Torr, a thin layer (10 nm) of MoO_3 was then thermally deposited as the anode interlayer, followed by thermal deposition of 100 nm Ag as the top electrode through a shadow mask. The active area of all devices was 0.07 cm^2. The *J-V* curves were measured on a computer-controlled Keithley 2400 source meter under 1 sun, the AM 1.5 G spectra came from a class solar simulator (Enlitech), and the light intensity was 100 $mWcm^{-2}$ as calibrated by a China General Certification Center-certified reference monocrystal silicon cell (Enlitech).

Please cite this article in press as: Yuan et al., Single-Junction Organic Solar Cell with over 15% Efficiency Using Fused-Ring Acceptor with Electron-Deficient Core, Joule (2019), https://doi.org/10.1016/j.joule.2019.01.004

Before the *J-V* test, a physical mask with an aperture with precise area of 0.04 cm^2 was used to define the device area.

Device characterization was carried out under AM 1.5G irradiation with the intensity of 100 mW cm^{-2} (Oriel 67005, 500 W), calibrated by a standard silicon cell. *J-V* curves were recorded with a Keithley 236 digital source meter. A xenon lamp with AM 1.5 filter was used as the white light source and the optical power was 100 mW cm^{-2}. The *EQE* measurements of organic solar cells were performed by Stanford Systems model SR830 DSP lock-in amplifier coupled with WDG3 monochromator and 500 W xenon lamp. A calibrated silicon detector was used to determine the absolute photosensitivity at different wavelengths. All of these fabrications and characterizations were conducted in a glove box.

The Certificated PCE of the Devices

Test Method

The certification was performed by Enli Tech Optoelectronic Calibration Lab, which is accredited by Taiwan Accreditation Foundation (TAF) to ISO/IEC 17025. TAF is a full member of ILAC MRA (International Laboratory Accreditation Cooperation Mutual Recognition Arrangement) and IAF MLA (International Accreditation Forum Multilateral Recognition Arrangement). The testing of the sample was performed at standard testing conditions (STC) in accordance with IEC 60904-1:2006 Photovoltaic devices – Part 1: Measurement of photovoltaic current-voltage characteristics and test standard operation procedure of maximum power measurement of solar cells under the irradiation with a steady-state class AAA solar simulator according to IEC 60904-9:2007 Photovoltaic devices – part 9: Solar simulator performance requirements. The spectral mismatch is calculated according to IEC 60904-7:2008 Photovoltaic devices – Part 7: Computation of the spectral mismatch correction for measurements of photovoltaic devices. The spectrum of the solar simulator is measured with a spectroradiometer. The spectral responsivity (or quantum efficiency) of the device under test is measured with a grating monochromatic according to IEC 60904-8:2014 Photovoltaic devices – Part 8: Measurement of spectral responsivity of a photovoltaic (PV) device.

The Details of Testing Procedures

The device under test (DUT) was an organic polymer solar cell. Each sample had 3 devices on one glass substrate. The device contact structure was of superstrate type. The active area of DUT was covered with an area-calibrated metal shadow mask. Before the measurement of current and voltage, the spectral responsivity (or quantum efficiency) was measured according to IEC60904-8:2014. The traceability to SI units was achieved by using a calibrated photodetector (ISO/IEC 17025, lab calibrated and traceable to NIST). The spectral mismatch correction factor, MMF, was calculated based on IEC 60904-7:2008. The temperature was controlled with the simulator's mechanical shutter and a TE air-cooler with an RTD temperature sensor to achieve STC. The current and voltage data were taken by Keithley 2400 SMU with ISO/IEC 17025:2005 calibration report (no. K1509300201, traceable to NML). Kelvin Probe 4-wire connection method was adopted to remove all wire resistance in the circuit loop, which may affect the current and fill-factor accuracy of test results. The model of solar simulator is SS-F5-3A. The 1-sun intensity of SS-F5-3A was set by the WPVS-type reference cell with KG5 optical filter, which is calibrated by NREL (NREL calibration no. 1239.02, NIST traceability) and corrected by the MMF calculated before. The spectroradiometer (model: SPR-3011-SP; ISO/IEC 17025, lab calibrated and traceable to NML) was used to measure and monitor the spectrum of solar simulator.

Hole Mobility and Electron Mobility Measurements

The hole-only or electron-only diodes were fabricated using the following architectures: ITO/PEDOT:PSS/active layer/gold (Au) for holes and ITO/ZnO/active layer/PDINO/Al for electrons. Mobilities were extracted by fitting the current density-voltage curves using the Mott-Gurney relationship (space charge limited current). The mobilities were obtained by taking current-voltage curves and fitting the results to a space charge limited form.

Grazing Incidence Wide-Angle and Small-Angle X-Ray Scattering Measurements

GIWAXS and GISAXS measurements were carried out with a Xeuss 2.0 SAXS/WAXS laboratory beamline using a Cu X-ray source (8.05 keV, 1.54 Å) and a Pilatus3R 300K detector. The incidence angle is 0.2°. All measurements were conducted under a vacuum environment to reduce air scattering.

Atomic Force Microscopy and Transmission Electron Microscopy

The morphologies of the polymer/acceptor blend films were investigated by AFM (Agilent Technologies, 5500 AFM/SPM System) in contacting under normal air conditions at room temperature with a 1 μm, 3 μm, and 5 μm scanner. Samples for the TEM measurements were prepared as follows: the active layer films were spin-casted on ITO/poly(3,4-ethylenedioxythiophene) poly(styrenesulfonate) (PEDOT:PSS) substrates, and the substrates with active layers were submerged in deionized water to make the active layers float onto the air-water interface. Then, the floated films were picked up on an unsupported 200 mesh copper grid for the TEM measurements. TEM measurements were performed in a JEM-2100F.

Calculations

DFT calculations were performed with the ωB97X-D functional using the 6-31+G(d,p) basis set.[2] Gaussian 16, revision B.010 was used for all calculations.[3] The molecule Y6 was studied, with the N-alkyl chains replaced with N-secButyl groups, and the side alkyl chains replaced with $-CH_3$. The geometry of Y6 was optimized and the vibrational frequencies were verified.

SUPPLEMENTAL INFORMATION

Supplemental Information includes Supplemental Experimental Procedures, 25 figures, and 11 tables and can be found with this article online at https://doi.org/10.1016/j.joule.2019.01.004.

ACKNOWLEDGMENTS

Y. Zou acknowledges the National Key Research & Development Projects of China (2017YFA0206600), National Natural Science Foundation of China (21875286), and Science Fund for Distinguished Young Scholars of Hunan Province (2017JJ1029). Y.L. thanks the financial support of NSFC (91633301). H.-L.Y. acknowledges the National Natural Science Foundation of China (21761132001 and 91633301). X.L. acknowledges the financial support from CUHK direct grant and NSFC/RGC Joint Research Scheme (grant no. N_CUHK418/17), and M.L. and P.A.J. acknowledge financial support from NSERC, CIFAR, and Sentinelle Nord. This research was enabled in part by Calcul Québec, Compute Ontario, SHARCNET, and Compute Canada.

AUTHOR CONTRIBUTIONS

J.Y. and Y. Zou conceived the idea; J.Y., Y. Zou, and Y. Zhang designed the synthetic route of the small-molecule acceptor and synthesized the molecule, and carried out

the NMR and high-resolution mass spectrum measurements, and ultraviolet and cyclic voltammetry; L.Z. fabricated the conventional solar cell devices and performed the atomic force microscopy and TEM supervised by Y. Zou and Y.L.; T.-K.L. performed the GIWAXS and GISAXS experiment supervised by X.L.; G.Z. fabricated the inverted solar cell devices and performed the *IQE* experiments under the supervision of H.-L.Y.; P.A.J. and M.L. performed theoretical calculations of the small-molecule acceptor; J.Y. wrote the original draft; and all authors, including C.Z., H.P., Y.C., and J.U., contributed to analysis and writing.

DECLARATION OF INTERESTS

The authors declare no competing interests.

Received: October 30, 2018
Revised: December 5, 2018
Accepted: January 10, 2019
Published: January 17, 2019

REFERENCES

1. Yu, G., Gao, J., Hummelen, J.C., Wudl, F., and Heeger, A.J. (1995). Polymer photovoltaic cells - enhanced efficiencies via a network of internal donor-acceptor heterojunctions. Science *270*, 1789–1791.

2. Halls, J.J.M., Pichler, K., Friend, R.H., Moratti, S.C., and Holmes, A.B. (1996). Exciton diffusion and dissociation in a poly(p-phenylenevinylene)/C60 heterojunction photovoltaic cell. Appl. Phys. Lett. *68*, 3120–3122.

3. Thompson, B.C., and Fréchet, J.M. (2008). Polymer-fullerene composite solar cells. Angew. Chem. Int. Ed. *47*, 58–77.

4. Li, G., Zhu, R., and Yang, Y. (2012). Polymer solar cells. Nat. Photonics *6*, 153–161.

5. Li, Y., and Zou, Y. (2008). Conjugated polymer photovoltaic materials with broad absorption band and high charge carrier mobility. Adv. Mater. *20*, 2952–2958.

6. Li, C., Liu, M., Pschirer, N.G., Baumgarten, M., and Müllen, K. (2010). Polyphenylene-based materials for organic photovoltaics. Chem. Rev. *110*, 6817–6855.

7. Qian, D., Zheng, Z., Yao, H., Tress, W., Hopper, T.R., Chen, S., Li, S., Liu, J., Chen, S., Zhang, J., et al. (2018). Design rules for minimizing voltage losses in high-efficiency organic solar cells. Nat. Mater. *17*, 703–709.

8. Liu, Y., Zhao, J., Li, Z., Mu, C., Ma, W., Hu, H., Jiang, K., Lin, H., Ade, H., and Yan, H. (2014). Aggregation and morphology control enables multiple cases of high-efficiency polymer solar cells. Nat. Commun. *5*, 5293.

9. Huang, Y., Kramer, E.J., Heeger, A.J., and Bazan, G.C. (2014). Bulk heterojunction solar cells: morphology and performance relationships. Chem. Rev. *114*, 7006–7043.

10. Hu, H., Chow, P.C.Y., Zhang, G., Ma, T., Liu, J., Yang, G., and Yan, H. (2017). Design of donor polymers with strong temperature-dependent aggregation property for efficient organic photovoltaics. Acc. Chem. Res. *50*, 2519–2528.

11. Zhao, W., Li, S., Yao, H., Zhang, S., Zhang, Y., Yang, B., and Hou, J. (2017). Molecular optimization enables over 13% efficiency in organic solar cells. J. Am. Chem. Soc. *139*, 7148–7151.

12. Lin, Y., Wang, J., Zhang, Z.G., Bai, H., Li, Y., Zhu, D., and Zhan, X. (2015). An electron acceptor challenging fullerenes for efficient polymer solar cells. Adv. Mater. *27*, 1170–1174.

13. Luo, Z., Bin, H., Liu, T., Zhang, Z.G., Yang, Y., Zhong, C., Qiu, B., Li, G., Gao, W., Xie, D., et al. (2018). Fine-tuning of molecular packing and energy level through methyl substitution enabling excellent small molecule acceptors for nonfullerene polymer solar cells with efficiency up to 12.54. Adv. Mater. *30*, 1706124.

14. Xu, X., Bi, Z., Ma, W., Wang, Z., Choy, W.C.H., Wu, W., Zhang, G., Li, Y., and Peng, Q. (2017). Highly efficient ternary-blend polymer solar cells enabled by a nonfullerene acceptor and two polymer donors with a broad composition tolerance. Adv. Mater. *29*, 1704271.

15. Zhou, Y., Kurosawa, T., Ma, W., Guo, Y., Fang, L., Vandewal, K., Diao, Y., Wang, C., Yan, Q., Reinspach, J., et al. (2014). High performance all-polymer solar cell via polymer side-chain engineering. Adv. Mater. *26*, 3767–3772.

16. Baran, D., Ashraf, R.S., Hanifi, D.A., Abdelsamie, M., Gasparini, N., Röhr, J.A., Holliday, S., Wadsworth, A., Lockett, S., Neophytou, M., et al. (2017). Reducing the efficiency-stability-cost gap of organic photovoltaics with highly efficient and stable small molecule acceptor ternary solar cells. Nat. Mater. *16*, 363–369.

17. Li, Y., Lin, J.D., Che, X., Qu, Y., Liu, F., Liao, L.S., and Forrest, S.R. (2017). High efficiency near-infrared and semitransparent non-fullerene acceptor organic photovoltaic cells. J. Am. Chem. Soc. *139*, 17114–17119.

18. Meng, D., Sun, D., Zhong, C., Liu, T., Fan, B., Huo, L., Li, Y., Jiang, W., Choi, H., Kim, T., et al. (2016). High-performance solution-processed non-fullerene organic solar cells based on selenophene-containing perylene bisimide acceptor. J. Am. Chem. Soc. *138*, 375–380.

19. Wu, Q., Zhao, D., Schneider, A.M., Chen, W., and Yu, L. (2016). Covalently bound clusters of alpha-substituted PDI-rival electron acceptors to fullerene for organic solar cells. J. Am. Chem. Soc. *138*, 7248–7251.

20. Yao, Z., Liao, X., Gao, K., Lin, F., Xu, X., Shi, X., Zuo, L., Liu, F., Chen, Y., and Jen, A.K. (2018). Dithienopicenocarbazole-based acceptors for efficient organic solar cells with optoelectronic response over 1000 nm and an extremely low energy loss. J. Am. Chem. Soc. *140*, 2054–2057.

21. Ma, Y., Zhang, M., Yan, Y., Xin, J., Wang, T., Ma, W., Tang, C., and Zheng, Q. (2017). Ladder-type dithienonaphthalene-based small-molecule acceptors for efficient nonfullerene organic solar cells. Chem. Mater. *29*, 7942–7952.

22. Liu, Y., Zhang, Z., Feng, S., Li, M., Wu, L., Hou, R., Xu, X., Chen, X., and Bo, Z. (2017). Exploiting noncovalently conformational locking as a design strategy for high performance fused-ring electron acceptor used in polymer solar cells. J. Am. Chem. Soc. *139*, 3356–3359.

23. Xia, D., Gehrig, D., Guo, X., Baumgarten, M., Laquai, F., and Müllen, K. (2015). A spiro-bifluorene based 3D electron acceptor with dicyanovinylene substitution for solution-processed non-fullerene organic solar cells. J. Mater. Chem. A Mater. Energy Sustain. *3*, 11086–11092.

24. Jiang, W., Yu, R., Liu, Z., Peng, R., Mi, D., Hong, L., Wei, Q., Hou, J., Kuang, Y., and Ge, Z. (2018). Ternary nonfullerene polymer solar cells with 12.16% efficiency by introducing one acceptor with cascading energy level and complementary absorption. Adv. Mater. *30*, 1703005.

25. Kan, B., Zhang, J., Liu, F., Wan, X., Li, C., Ke, X., Wang, Y., Feng, H., Zhang, Y., Long, G., et al. (2018). Fine-tuning the energy levels of a nonfullerene small-molecule acceptor to achieve a high short-circuit current and a power

conversion efficiency over 12% in organic solar cells. Adv. Mater. *30*, 1704904.

26. Guo, X., Facchetti, A., and Marks, T.J. (2014). Imide- and amide-functionalized polymer semiconductors. Chem. Rev. *114*, 8943–9021.

27. Cheng, P., Li, G., Zhan, X., and Yang, Y. (2018). Next-generation organic photovoltaics based on non-fullerene acceptors. Nat. Photonics *12*, 131–142.

28. Zhang, S., Qin, Y., Zhu, J., and Hou, J. (2018). Over 14% efficiency in polymer solar cells enabled by a chlorinated polymer donor. Adv. Mater. *30*, e1800868.

29. Fei, Z., Eisner, F.D., Jiao, X., Azzouzi, M., Rohr, J.A., Han, Y., Shahid, M., Chesman, A.S.R., Easton, C.D., McNeill, C.R., et al. (2018). An alkylated indacenodithieno[3,2-b]thiophene-based nonfullerene acceptor with high crystallinity exhibiting single junction solar cell efficiencies greater than 13% with low voltage losses. Adv. Mater. *30*, 1705209.

30. Li, W., Ye, L., Li, S., Yao, H., Ade, H., and Hou, J. (2018). A High-efficiency organic solar cell enabled by the strong intramolecular electron push-pull effect of the nonfullerene acceptor. Adv. Mater. *30*, e1707170.

31. Sun, J., Ma, X., Zhang, Z., Yu, J., Zhou, J., Yin, X., Yang, L., Geng, R., Zhu, R., Zhang, F., and Tang, W. (2018). Dithieno[3,2-b:2′,3′-d]pyrrol fused nonfullerene acceptors enabling over 13% efficiency for organic solar cells. Adv. Mater. *30*, e1707150.

32. Zhou, Z., Xu, S., Song, J., Jin, Y., Yue, Q., Qian, Y., Liu, F., Zhang, F., and Zhu, X. (2018). High-efficiency small-molecule ternary solar cells with a hierarchical morphology enabled by synergizing fullerene and non-fullerene acceptors. Nat. Energy *3*, 952–959.

33. Wang, J., Zhang, J., Xiao, Y., Xiao, T., Zhu, R., Yan, C., Fu, Y., Lu, G., Lu, X., Marder, S.R., and Zhan, X. (2018). Effect of isomerization on high-performance nonfullerene electron acceptors. J. Am. Chem. Soc. *140*, 9140–9147.

34. Huang, C., Liao, X., Gao, K., Zuo, L., Lin, F., Shi, X., Li, C.-Z., Liu, H., Li, X., Liu, F., et al. (2018). Highly efficient organic solar cells based on S,N-heteroacene non-fullerene acceptors. Chem. Mater. *30*, 5429–5434.

35. Zhang, M., Guo, X., Ma, W., Ade, H., and Hou, J. (2015). A large-bandgap conjugated polymer for versatile photovoltaic applications with high performance. Adv. Mater. *27*, 4655–4660.

36. Rühle, S. (2016). Tabulated values of the Shockley–Queisser limit for single junction solar cells. Sol. Energy *130*, 139–147.

37. Feng, L., Yuan, J., Zhang, Z., Peng, H., Zhang, Z.G., Xu, S., Liu, Y., Li, Y., and Zou, Y. (2017). Thieno[3,2-b]pyrrolo-fused pentacyclic benzotriazole-based acceptor for efficient organic photovoltaics. ACS Appl. Mater. Interfaces *9*, 31985–31992.

38. Wu, J.S., Cheng, S.W., Cheng, Y.J., and Hsu, C.S. (2015). Donor-acceptor conjugated polymers based on multifused ladder-type arenes for organic solar cells. Chem. Soc. Rev. *44*, 1113–1154.

39. Hu, H., Jiang, K., Yang, G., Liu, J., Li, Z., Lin, H., Liu, Y., Zhao, J., Zhang, J., Huang, F., et al. (2015). Terthiophene-based D-A polymer with an asymmetric arrangement of alkyl chains that enables efficient polymer solar cells. J. Am. Chem. Soc. *137*, 14149–14157.

40. Park, S.H., Roy, A., Beaupré, S., Cho, S., Coates, N., Moon, J.S., Moses, D., Leclerc, M., Lee, K., and Heeger, A.J. (2009). Bulk heterojunction solar cells with internal quantum efficiency approaching 100%. Nat. Photonics *3*, 297–302.

41. Chen, Z., Cai, P., Chen, J., Liu, X., Zhang, L., Lan, L., Peng, J., Ma, Y., and Cao, Y. (2014). Low band-gap conjugated polymers with strong interchain aggregation and very high hole mobility towards highly efficient thick-film polymer solar cells. Adv. Mater. *26*, 2586–2591.

42. Lei, T., Xia, X., Wang, J.Y., Liu, C.J., and Pei, J. (2014). "Conformation locked" strong electron-deficient poly(p-phenylene vinylene) derivatives for ambient-stable n-type field-effect transistors: synthesis, properties, and effects of fluorine substitution position. J. Am. Chem. Soc. *136*, 2135–2141.

43. Uddin, M.A., Lee, T.H., Xu, S., Park, S.Y., Kim, T., Song, S., Nguyen, T.L., Ko, S.-j., Hwang, S., Kim, J.Y., and Woo, H.Y. (2015). Interplay of intramolecular noncovalent coulomb interactions for semicrystalline photovoltaic polymers. Chem. Mater. *27*, 5997–6007.

44. Huang, H., Yang, L., Facchetti, A., and Marks, T.J. (2017). Organic and polymeric semiconductors enhanced by noncovalent conformational locks. Chem. Rev. *117*, 10291–10318.

45. Zhang, Z., Yu, J., Yin, X., Hu, Z., Jiang, Y., Sun, J., Zhou, J., Zhang, F., Russell, T.P., Liu, F., and Tang, W. (2018). Conformation locking on fused-ring electron acceptor for high-performance nonfullerene organic solar cells. Adv. Funct. Mater. *28*, 1705095.

46. Chai, J.-D., and Head-Gordon, M. (2008). Long-range corrected hybrid density functionals with damped atom-atom dispersion corrections. Phys. Chem. Chem. Phys. *10*, 6615–6620.

47. Frisch, M.J., Trucks, G.W., Schlegel, H.B., Scuseria, G.E., Robb, M.A., Cheeseman, J.R., Scalmani, G., Barone, V., Petersson, G.A., Nakatsuji, H., et al. (2016). Gaussian 16, Revision B.01 (Gaussian, Inc.).

48. Long, G., Wu, B., Solanki, A., Yang, X., Kan, B., Liu, X., Wu, D., Xu, Z., Wu, W.R., and Jeng, U.S. (2016). New insights into the correlation between morphology, excited state dynamics, and device performance of small molecule organic solar cells. Adv. Energy Mater. *6*, 1600961.

49. Yuan, J., Qiu, L., Zhang, Z.-G., Li, Y., Chen, Y., and Zou, Y. (2016). Tetrafluoroquinoxaline based polymers for non-fullerene polymer solar cells with efficiency over 9%. Nano Energy *30*, 312–320.

50. Liu, J., Chen, S., Qian, D., Gautam, B., Yang, G., Zhao, J., Bergqvist, J., Zhang, F., Ma, W., and Ade, H. (2016). Fast charge separation in a non-fullerene organic solar cell with a small driving force. Nat. Energy *1*, 16089.

51. Gong, X., Tong, M., Brunetti, F.G., Seo, J., Sun, Y., Moses, D., Wudl, F., and Heeger, A.J. (2011). Bulk heterojunction solar cells with large open-circuit voltage: electron transfer with small donor-acceptor energy offset. Adv. Mater. *23*, 2272–2277.

52. Rao, A., Chow, P.C.Y., Gélinas, S., Schlenker, C.W., Li, C.-Z., Yip, H.-L., Jen, A.K.Y., Ginger, D.S., and Friend, R.H. (2013). The role of spin in the kinetic control of recombination in organic photovoltaics. Nature *500*, 435–439.

53. Mai, J., Xiao, Y., Zhou, G., Wang, J., Zhu, J., Zhao, N., Zhan, X., and Lu, X. (2018). Hidden structure ordering along backbone of fused-ring electron acceptors enhanced by ternary bulk heterojunction. Adv. Mater. *30*, e1802888.